Energy and AI 13 (2023) 100254

Contents lists available at ScienceDirect

Energy and AI

journal homepage: www.sciencedirect.com/journal/energy-and-ai

Analysis of PEM and AEM electrolysis by neural network pattern recognition, association rule mining and LIME

M. Erdem Günay [a], N. Alper Tapan [b,*]

[a] Department of Energy Systems Engineering, Istanbul Bilgi University, Eyupsultan, Istanbul 34060, Turkey
[b] Department of Chemical Engineering, Gazi University, Maltepe, Ankara 06570, Turkey

HIGHLIGHTS

- ARM provided the dominant rules leading to high current density.
- LIME and neural network pattern recognition successfully uncovered the importance of catalytic , operational and material variables.

GRAPHICAL ABSTRACT

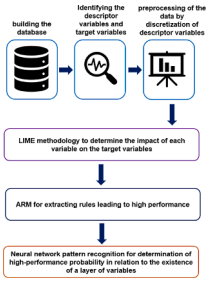

ARTICLE INFO

Keywords:
Machine learning
Data mining
Hydrogen production
Current density

ABSTRACT

In this work, as an extension of previous machine learning studies, three novel techniques, namely local interpretable model-agnostic explanations (LIME), neural network pattern recognition and association rule mining (ARM) were utilized for proton exchange membrane (PEM) and anion exchange membrane (AEM) electrolyzer database for hydrogen production. The main goal of LIME was to determine the positive or negative effects of a variety of descriptor variables on current density, power density and polarization. Using this technique, it was possible to uncover rules or paths that lead to high current density, low power density and low polarization. ARM provided the dominant rules leading to high current density such as using ELAT as the cathode gas diffusion layer, using pure Pt on the cathode surface and using pure carbon as the cathode support. In addition, LIME and neural network pattern recognition successfully uncovered the importance of catalytic materials such as cathode/anode support/surface elements, operational variables like K_2CO_3 or KOH concentration in the electrolyte, certain membrane types, gas diffusion layers, and applied potential on current density. It was then concluded that machine learning can help determine the ideal conditions for developing a PEM and AEM electrolyzer to maximize hydrogen generation, which can also guide future research.

1. Introduction

Artificial intelligence is a subfield of computer science and engineering that focuses on the development of smart or intelligent technologies, devices, and systems that can perform tasks that are analogous to human learning and decision-making [1]. It can also be

* Corresponding author.
E-mail address: atapan@gazi.edu.tr (N.A. Tapan).

https://doi.org/10.1016/j.egyai.2023.100254

Available online 13 March 2023

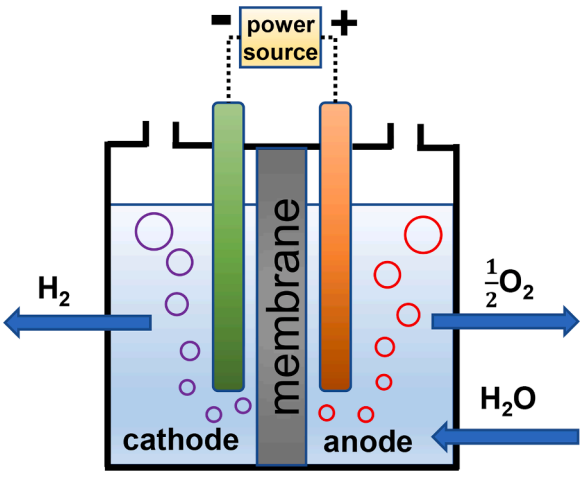

Fig. 1. Schematic representation of PEM electrolyzer [17].

defined as the capacity of a system to correctly comprehend external information, to learn from that knowledge, and to use those learnings to achieve specific goals and tasks over flexible adaptation. Machine learning is a subfield of artificial intelligence that tries to design and optimize computer programs that can automatically learn from data collected in the past using algorithms and statistics. These applications can then be used to examine data sets, discover previously unseen trends and patterns, generalize information, create models, or extract heuristics-based rules [2]. Moreover, they have an exceptional capability for identifying nonlinear relationships between the input and output variables [3].

Machine learning has numerous applications in a variety of areas, and its use in the field of energy has increased dramatically in recent years. One example is the prediction of future (daily, monthly, or annual) energy, electricity or fuel consumption by methods like artificial neural networks [4–7] or support vector machines [8,9]. The use of machine learning methodologies in renewable energy technologies is also quite common as reviewed recently for solar energy [10], wind energy [11], geothermal energy [12], bioenergy [13] and hydrogen production [14].

Among these renewable energy technologies, hydrogen is a very good alternative energy source that only gives off only water when burned or used in fuel cells. Although hydrogen is the most abundant element in the universe, obtaining elemental hydrogen on earth is quite challenging. Thermochemical techniques like coal gasification, hydrocarbon reforming, plasma reforming, and hydrocarbon pyrolysis can be used to produce hydrogen, all of which rely on fossil fuels; whereas using electrolysis for splitting of water into hydrogen and oxygen is another option [15,16]. Even though it has been known for more than 200 years that water electrolysis can produce hydrogen, the efficient use of electrolyzers still needs a lot of scientific work to move to industrial stage [17]. Thanks to recent improvements in its technology and electrode materials, PEM electrolysis is still considered to be the greatest alternative for producing clean and pure hydrogen due to its sustainability and absence of carbon footprint. PEM electrolyzers have also distinct benefits over alkaline devices such that they are less caustic and reversible. Moreover, they are able to work at lower cell voltages, higher current densities, higher temperatures and higher pressures, resulting in better efficiencies (80-90%) [18]. PEM electrolyzers use electricity to oxidize water and on each side of the membrane and the electrochemical reactions take place in a porous catalyst layer (Fig. 1). Oxygen and protons are created at the anode, then, protons cross the membrane and electrons move through the external circuit, and the electrons at the cathode reduce the protons producing hydrogen.

In PEM and AEM electrolyzers, identification of complex rules or pathways that result in high current density, low power density, and low polarization may require the optimization of several variables such as support and surface elements, gas diffusion layers of both cathode and anode, membrane type, electrolyte type and flow rate, temperature etc. However, this task is too difficult to accomplish by conventional methods, due to the complex relationships of these variables with the performance of the electrolyzer. Here at this point, advanced modeling techniques and machine learning based methodologies can be applied to determine the best combination of variables leading to high performance as reviewed in a recently published paper [19]. Among the successful applications, Zhao et al. used dynamic hierarchical modeling and control for high-temperature PEM electrolyzer cell systems [20]. In addition, Mohamed et al. used five different machine learning algorithms (artificial neural networks, polynomial regression, support vector machine regressor, k-nearest neighbor regressor, and decision tree regressor) to predict hydrogen generation rate and current density [21]. On the other hand, the research conducted by Yin et al. focused on the applications of machine learning methodologies in membrane design and discovery [22]. As a final example, Kim et al. concentrated on creating optimal machine learning algorithms to understand the operational properties of PEM electrolyzers [23].

For this work, we prepared a database of 789 experimental data entries reported in 30 academic publications. With the help of this database, we were able to use and test a number of new and effective machine learning methods to find the best combination of variables leading to the highest efficiency. For instance, in our earlier research work, classification tree was used as a tool in order to generalize high-performance routes and determine important catalytic, materials or operational parameters by objectively gathering 10 years of polarization data from studies conducted by various research groups [17]. After hyperparameter optimization to minimize the classification error, 5 alternative paths to high current densities, 4 alternative paths to low power density and 2 alternative paths to low polarization were determined as tabulated in Fig. 2. As it is indicated in this figure, low polarization target requires only 4 variables which are current density,

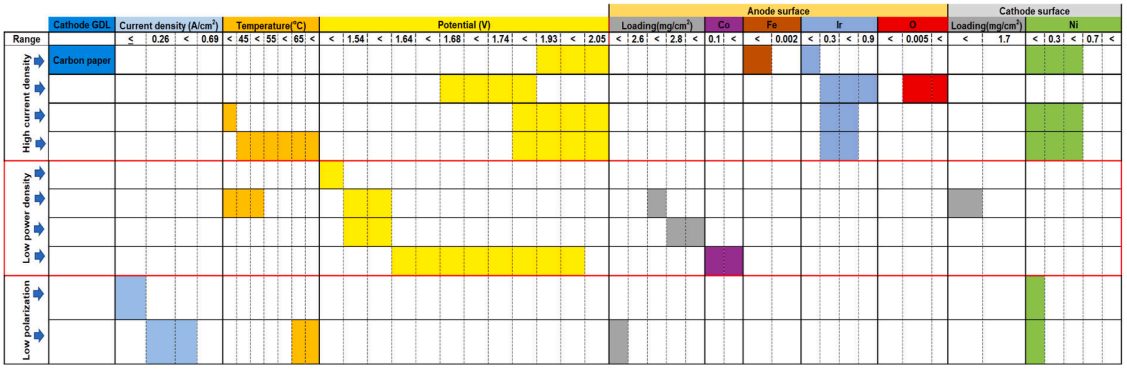

Fig. 2. Alternative parts leading to high performance variables extracted from classification trees [17].

Table 1
Ranges and types of input variables used in neural network pattern recognition and ARM (numbers in parenthesis refer to levels of that variable).

Descriptor variable	Ranges of continuous variables and identities of discrete variables
cathode support elements (feature layers 1-11)	B:0.0708 (1), Ce:0.0043 (2), La:0.0022 (3), O:0.015 (4), Mo:0.335 (5), P:0.0099 (6), S:0.665 (7), C:0.9292 (8), C:0.98 (9), C:0.99 (10), C:1 (11)
cathode support to surface ratio (feature layers 12-21)	4.76 (12), 10.84 (13), 12.83 (14), 16.26 (15), 19.08 (16), 20.84 (17), 24.39 (18), 37.93 (19), 39.38 (20), 65.03 (21)
cathode surface elements (feature layers 22-39)	Pt:0.51(22), Pt:1 (23), Ru:0.49 (24), Ru:0.335 (25), Al:0.66 (26), Pd:1 (27), O:0.571 (28), Fe:0.335 (29), Fe:0.33 (30), Co:0.43 (31), Co:0.335 (32), Co:0.33 (33), Mo:0.0717 (34), Ni:1 (35), Ni:0.335 (36), Ni:0.33 (37), Ni:0.269 (38), S:0.665 (39)
cathode catalyst loading (mg.cm^{-2}) (feature layers 40-61)	42.7 (40), 5 (41), 3.5 (42), 3 (43), 2.4 (44), 2.33 (45), 2.3 (46), 2 (47), 1.5 (48), 1.33 (49), 1.25 (50), 1.125 (51), 1.09 (52), 1 (53), 0.833 (54), 0.7 (55), 0.6 (56), 0.54 (57), 0.5 (58), 0.4 (59), 0.25 (60), 0.0085 (61)
cathode gas diffusion layer type (feature layers 62-81)	Toray C. P. (62), C. P. (model unspecified) (63), 34BC-SGL (64), TGP-H120 (65) 5wt%Tef.tr. TGP-H120 (66), ELAT (67), C.P.SGL (68), Bekipor-Ti.-2-28-0.7 (69), SS Fiber Paper (70), 3SS-5-050AN (71), 20wt%Tef.tr. TGP-H-090 (72), SSGPMF-4.25 (73), Ti.P.Sint. (74), Ti Part.Sint-50-1 (75), TGP-H-090 (76), Untr.TGP-090 (77), No spec. (Cat.) (78), H24C5 (79), C Cloth (80), NiFo (81)
anode support elements (feature layers 82-102)	Ir:1 (82), Al:0.4 (83), V:0.3 (84), V:0.2 (85), V:0.1 (86), Mo:0.1 (87), O:0.7 (88), O:0.64 (89), O:0.6 (90), O:0.53 (91), O:0.4 7(92), C:0.5 (93), Ti:1 (94), Ti:0.5 (95), Ti:0.36 (96), Ti:0.33 (97), Ti:0.3 (98), Ti:0.27 (99), Ti:0.23 (100),Ti:0.20 (101), Ni:1 (102)
anode support to surface ratio (feature layers 103-113)	0 (103), 1 (104), 1.4 (105), 1.87 (106), 2.57 (107), 5.35 (108), 8.53 (109), 9.12 (110), 9.92 (111), 11.4 (112), 17.46 (113)
anode surface elements (feature layers 114-159)	Ir:0.104 (114), Ir:0.3 (115), Ir:0.33 (116), Ir:0.335 (117), Ir:0.42 (118), Ir:0.7 (119), Ir:0.92 (120), Ir:1 (121), Ta:0.021 (122), C:0.597 (123), Pt:0.34 (124), O:0.7 (125), O:0.67 (126), O:0.66 (127), O:0.574 (128), O:0.571 (129), O:0.3 (130), O:0.08 (131), O:0.01 (132), Al:0.66 (133), Mo:0.07 (134), Ni:1 (135), Ni:0.27 (136), Ni:0.14 (137), Ni:0.09 (138), Li:0.03 (139), Cu:0.28 (140), Cu:0.14 (141), Cu:0.1 (142), Co:0.67 (143), Co:0.5 (144), Co:0.4 (145), Co:0.33 (146), Co:0.32 (147), Co:0.29 (148), Co:0.15 (149),Co:0.06 (150), Fe:0.67 (151), Fe:0.5 (152), Fe:0.33 (153), Fe:0.29 (154), Fe:0.004 (155), Ru:0.33 (156), Ru:0.31 (157), Ru:0.3 (158), Ru:0.18 (159)
anode catalyst loading (mg.cm^{-2}) (feature layers 160-193)	78.9 (160), 42.7 (161), 7.29 (162), 5 (163), 4.4 (164), 4.2 (165), 4.1 (166), 3.95 (167), 3 (168), 2.92 (169), 2.68 (170), 2.5 (171), 2.2 (172), 2 (173), 1.91 (174), 1.5 (175), 1.4 (176), 1.125 (177), 1 (178), 0.9 (179), 0.71 (180), 0.69 (181), 0.64 (182), 0.51 (183), 0.50 (184), 0.48 (185), 0.47 (186), 0.4 (187), 0.23 (188), 0.22 (189), 0.18 (190), 0.12 (191), 0.1 (192), 0.0085 (193)
anode gas diffusion layer type (feature layers 194-215)	Bekipor® ST Titanium Grade 1 felts with 68% porosity(194), BEKIPOR® Titanium-2 GDL 28 - 0.7 (microporous gas diffusion layer)(195), Ti diffusion layer (Bekaert) (196), Nickel Fiber Paper (197), Bekaert 2GDL40-1.0 Ti felt (198), Carbon Cloth (199), Sintered Ti Particles (50 mm Pore Diameter, 1 mm Thickness) (200), Ti Felt (201), PTL 4 - Fibrous Ti-Sinter (Porosity % 67.61) (202), SS Gradient Porous Metal Framework (GPMF, 4.25 mm Thickness) (203), No Gas Diffusion Layer (204), Ti Mesh (205), Titanium Fibre Mesh (Bekaert Toko Metal Fiber Co.) (206), Ir coated Bekipor® ST Titanium Grade 1 felts with 68% Porosity (207), Pt Coated Titanium Fibre Mesh (208), Pt-Coated (1 μg cm−2) Sintered Titanium Frit (400 μm Thickness) (209), Porous titanium disc made of sintered powder (APT Co.) (210), Ni Foam (211), TGPH-030Toray (212), TGPH-090 Toray (213), Stainless Steel Fiber Paper (214) ,TGPH-120 Toray (215).
electrolyte type (feature layers 216-223)	H_2O (conc) (M):55.56 (216), H_2O (conc) (M):55.55 (217), H_2O (conc) (M):55.33 (218), H_2O (conc) (M):54.09 (219), H_2O (conc) (M):53.126 (220), KOH (conc) (M):1 (221), K_2CO_3 (conc) (M):0.769 (222), K_2CO_3 (conc) (M):0.073 (223)
flowrate of electrolytes (ml.min^{-1}) (feature layers 224-235)	0.5 (224), 1 (225), 2 (226), 3.30 (227), 4 (228), 20 (229), 25 (230), 40 (231), 50 (232), 60 (233), 80 (234), 500 (235)
membrane type (feature layers 236-251)	Aqivion (E98-09S) (236), Aquivion (E98-05S) (237), Sustanion (238), Cranfield Membrane (which has quaternary ammonium function groups and synthesized by radiation grafting) (239), Aqivion (E100-09S) (240), N112 (241), N115 (242), N115CS (243), N117 (244), N212 (245), Nafion membrane (model unspecified) (246), FAA-3-50 (Fumapem) (247), FAA-3 (Fuma Tech) (248), HMT-PMBI (249), A-201 (Tokuyama) (250), Polibenzimidazol (PBI) (251)
potential (V) (layers 252-275)	3.1 (252), 3 (253), 2.8 (254), 2.6 (255), 2.5 (256), 2.4 (257), 2.3 (258), 2.2 (259), 2.1 (260), 2 (261), 1.9 (262), 1.8 (263), 1.7 (264), 1.6 (265), 1.5 (266), 1.4 (267), 1.3 (268), 1.2 (269), 1.1 (270), 1 (271), 0.9 (272), 0.8 (273), 0.7 (274), 0.6 (275)
temperature (°C) (layers 276-292)	150°C (276), 140°C (277), 130°C (278), 120°C (279), 110°C (280), 90°C (281), 80°C (282), 70°C (283), 60°C (284), 55°C (285), 50°C (286), 45°C (287), 40°C (288), 30°C (289), 28°C (290), 25°C (291), 20°C (292)

temperature, anode loading and cathode Ni mole fraction. The only variable which is dominant or frequent in the routes of low polarization, high current and power density is found as operating temperature. It is also seen in Fig. 2 that anode surface elements and cathode surface elements in high performance routes are used in both PEM and AEM electrolyzers.

In this previous study, machine learning was applied to general electrolyzer literature without the exclusion of alkaline or acidic systems. In other words, neither AEM nor PEM electrolyzer systems were eliminated in order to determine whether one type of electrolyzer is superior to the other. Therefore, the paths extracted from classification trees involve catalysts and materials in different pH environments. In the case of alkaline electrolysis, as an alternative to noble metals, non-noble metals can be effectively used as oxygen and hydrogen evolution catalysts [24]. Co, Fe surface anode elements which were predicted in high performance routes in Fig. 2 are generally used as oxygen evolution catalyst components [25–30] and Ni as in the form of alloys with other transition metals, oxides or as porous structures is generally used as hydrogen evolution catalyst in alkaline water electrolyzers [28,31–34]. Ru and Ir, on the other hand, are usually chosen in PEM electrolyzers due to their higher electrocatalytic activity or superior stability in the form of oxides and mixed oxides or as supported for oxygen evolution and carbon supported or unsupported Pt for hydrogen evolution [24, 35–47].

Of course, there are numerous techniques in the field of machine learning (other than classification trees) which may open different perspectives for the interpretation of the database. Therefore, in our most recent study, we decided to apply novel machine learning techniques like Shapley analysis, k-nearest neighbor classification and

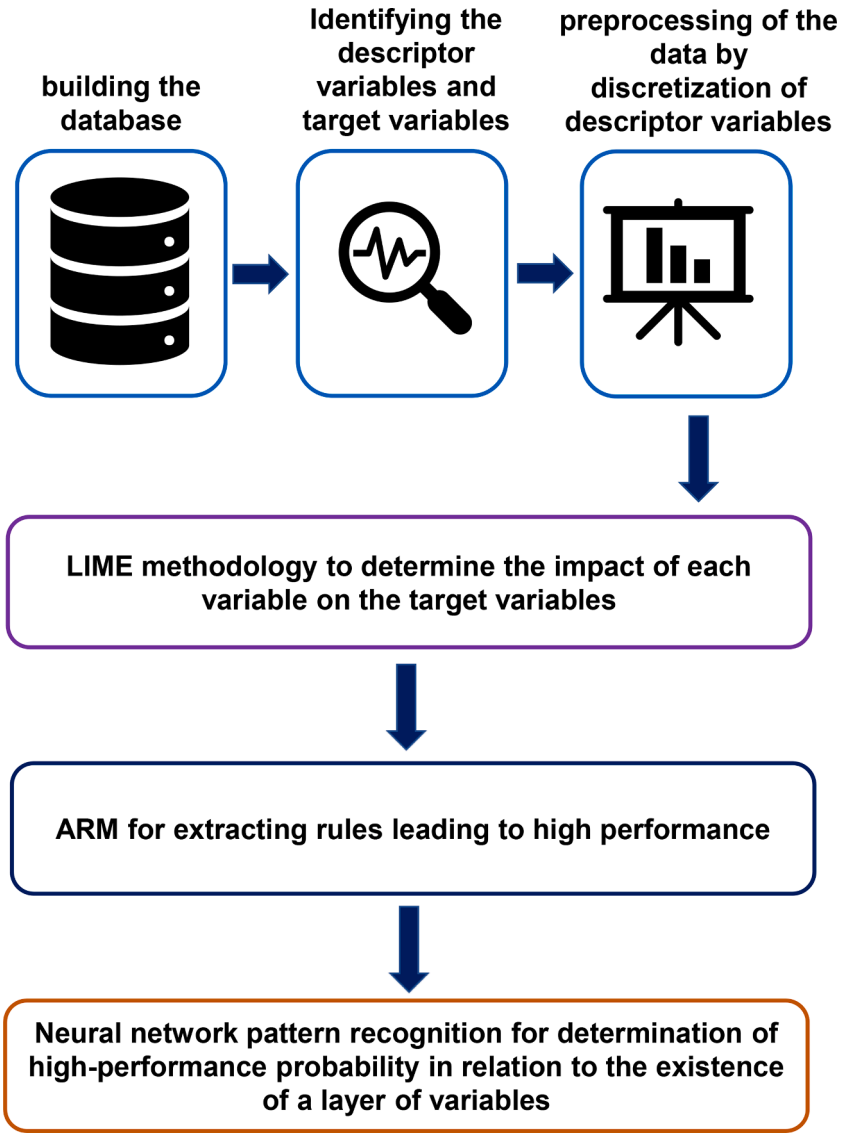

Fig. 3. Framework of the computational techniques.

Bayesian optimization on electrolyzer database [48]. As a result of this study, very specific effects of cathode support, surface and anode support, surface elements and operating variables on performance variables were determined like the positive effect of C, S or Mo (support elements) or Pt, Fe, Al, Ru, Co and S (surface elements) or the decrease in electrolyte flowrate on current density by Shapley analysis. In addition, as an optimum model in that study, k-nearest neighbor classification model successfully revealed the full effect of continuous and categorical features on current, power density and polarization. Furthermore, one interesting novel approach that was applied in our most recent work was Bayesian optimization used for designing future experiments by the use of small training set of observations. This probabilistic approach assisted to reach the optimum performance earlier and with minimum number of experiments with the same frequency of observation data set.

In the current study, different from our previous works, first, as a part of explainable machine learning, local interpretable model-agnostic explanations (LIME) method [49], was utilized in order to discover and evaluate the magnitude of the influence of each variable on current density, power density and polarization. As machine learning expands into more sensitive areas of research and has a broader range of applications in human daily life, explanations of machine learning algorithms using techniques like as LIME are becoming increasingly important. Accordingly, techniques like LIME can be applied to any machine learning model used in scientific environment [50–52]. Local surrogate models, such as LIME, are interpretable models that are used to explain individual predictions of black box machine learning algorithms [53]. The LIME method involves perturbing the input data and observing the output of the black-box model to determine how predictions change [54]. The output of LIME is a list of explanations that show how changes in each feature affects the prediction of a data sample.

Then, ARM was used for current density to find and extract hidden correlations between attributes in the database. In fact, there are many applications of association rule mining ranging from marketing to bioinformatics [55], food chemistry [56] or like in this study electrochemical engineering. ARM is a method that assists in identifying variables that appear "together" in a large dataset. Because one of those qualities could be the level of output variables (such as high current density) and the others are attributes characterizing the electrolyzer (such as cathode support elements), the technique may help to relate some attributes to the intended output [2]. The algorithms related to ARM are reviewed elsewhere [57].

Finally, neural network pattern recognition was implemented to model the relationship between existence of categorized electrochemical features and probability of high-performance variable (high

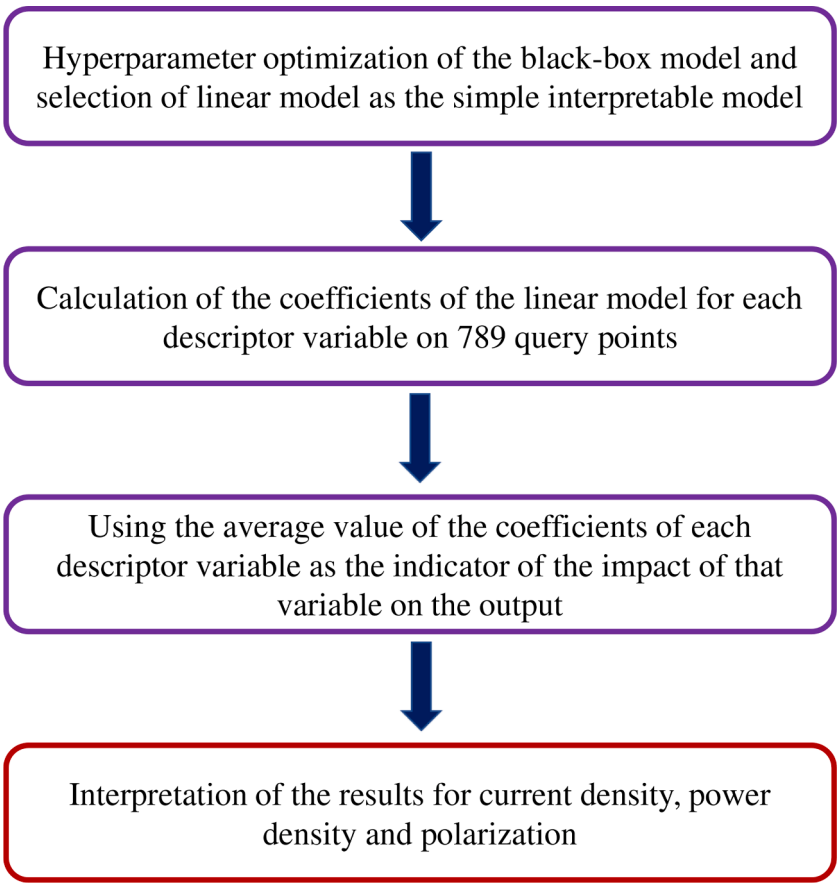

Fig. 4. Flow chart for LIME methodology.

current density) and to visualize hidden patterns. In fact , pattern recognition which is used to extract regularities and similarities in the database using machine learning techniques like artificial neural networks (ANN) have wide range of application areas ranging from speech processing, computer vision, robotics to medical diagnosis and finance [58]. Processed data after pattern recognition contain characteristic information with predicted values or probabilities for all features.

2. Methods and materials

2.1. Data

For this study, a database was constructed by gathering information from the literature on PEM and AEM electrolyzer materials. Even though the database was built from hundreds of scientific articles at first, only articles published in the last 10 years were used to get the data. This was done so that the database would be in accordance with current trends in this field. Because it is necessary to have a database that is completely defined in order to apply machine learning techniques, the articles that were lacking data were eventually ignored.

We have to also point out that some special elements like vanadium in our electrolyzer database can be observed. Indeed, vanadium can be used as a dopant on titania which is a very common support material for anode in PEM electrolyzer. In addition, vanadium is very well known for its redox properties and oxygenated species [59,60] which was utilized for oxygen evolution performance of anode electrode [36]. Therefore, vanadium is used in the support as a very common transition metal.

As a result, 30 papers were pooled together to make up a large enough statistically significant sample. Accordingly, 789 data items for 107 descriptor variables were divided into 292 categories for the use in machine learning techniques, as shown in Table 1. More information on the database can be found elsewhere [17].

2.2. Computational details

In this work, after identifying the descriptors and target variables, and preprocessing the database, LIME methodology was first applied to determine the impact of each variable on the target variables. Then, ARM was utilized for extracting rules leading to high performance and finally, neural network pattern recognition was employed for determination of high-performance probability in relation to the existence of a layer of variables. The computational framework is shown in Fig. 3.

LIME examines what happens to the predictions when varying the input data for a machine learning model [49]. LIME generates an explanation list that summarizes how each attribute helped in the prediction of a given data sample. This enables for local interpretability and the identification of which alterations to features will have the greatest effect on the prediction [53,54]. In this work, the codes related to LIME was written under MATLAB 2022a environment. As the blackbox model artificial neural networks were built while linear model was chosen as the simple interpretable model. The parameters of the artificial neural network were optimized with the options 'OptimizeHyperparameters', 'all' and then LIME was run over each query point. The coefficients of the variables on each query point were recorded and the average values of the coefficients were used as the indicator of impact on the output variable. The results were interpreted such that, a variable with a positive average coefficient has a positive effect on the target variable, while a variable with a negative average coefficient has a negative effect on the target. In addition, the impact of a variable on the output is proportional to the size of the average coefficients, with a larger average coefficient indicating a greater impact. In this study, LIME technique was performed to determine the effect of catalytic (surface and support

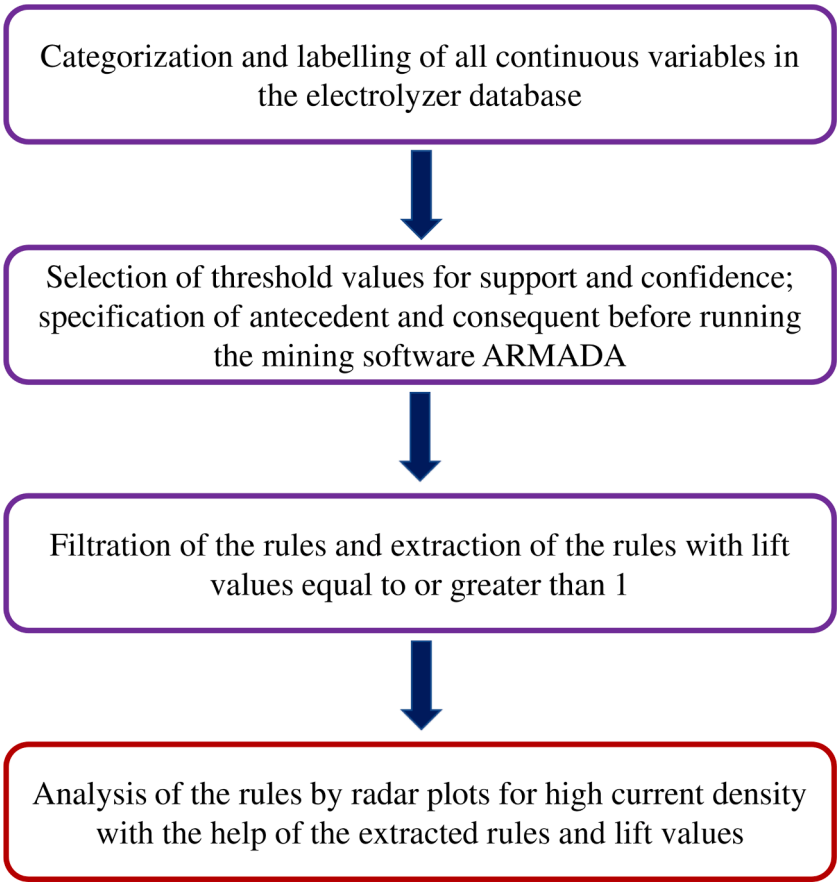

Fig. 5. Flow chart for association rule mining.

elemental compositions), material (membrane or gas diffusion layer type etc.) or operational variables (temperature, flow rate etc.) on current/power density and polarization. The flow chart for LIME methodology can be seen in Fig. 4.

After LIME analysis, ARM was utilized in order to reveal hidden rules behind electrolyzer database leading to high performance. The apriori algorithm in ARM with thresholds of support and confidence percentages was used to determine most frequent conditions of catalytic, material and operational variables combined in rules leading to high electrolyzer performance output which was selected as current density. Before application of association rule mining by ARMADA Data Mining Software (version 1.4), all continuous variables were categorized and labeled with specific numbers and antecedents as all electrolyzer input variables and consequents as high current density output were specified before running the mining software. The flow chart for the procedure of association rule mining can be seen in Fig. 5.

As an unsupervised machine learning technique, ARM was applied on the layered and categorized data set shown in Table 1. The aim in ARM was to determine the most frequent item sets whose conditions were set by a minimum threshold support and confidence of 10% of observation set and by goals of setting antecedents and consequents in the dataset. The fraction of layer(s) (or level of input variables) that yields high current density range is referred to as support of the rule. The ratio of frequency of high current density range at that layer(s) (input variable(s)) to the frequency of data at those layers is called the confidence. Lift is the strength of the rule which is the ratio of support of the rule to the supports of all elements in that rule. Lift is a very important criteria for ARM which indicates negative and positive correlations between the antecedents and consequents in the rule. Lift values smaller than one indicates negative, greater than one indicates positive and strong relationship between antecedents and consequent [61,62]. After application of ARM, all extracted rules were analyzed by radar plots by the value of lift of the rules. For the mining algorithm, ARMADA Data Mining Software (version1.4) [63] was used. 127 rules were extracted with a maximum number of antecedents equal to 6.

Finally, neural network pattern recognition was employed for determination of high-performance probability in relation to the existence of a layer of variables. For the aim of recognition of patterns in the data by the machine unlike humans, artificial neural networks can be used to map or capture the hidden relationship between input and output patterns. The outcome of this process is in fact a generalization of the relationships by capturing mapping function between input and output variables in the observation dataset by training feedforward neural network. At the end of this supervised learning process, the input-output relation can be mapped and visualized like the knowing of human being handwritten letters with different visual properties [58]. The flowchart for neural network pattern recognition technique applied on our electrolyzer database can be seen in Fig. 6.

For the neural network pattern recognition, database that was constructed with 15 different types of groups and 107 catalytic, material and operational variables were separated into 292 categorical layers to be used in neural network pattern recognition. Current density was selected as the output variable and also separated into three equally distributed ranges as low, medium and high with the ranges as [0 to 0.2504], [0.2516 to 1] and [1.01 to 6] A/cm^2, respectively. From the data set of 789 observations, 10% were separated as unseen observations. The rest of the data set which consisted of 711 observations were used to determine the performance of the neural network model. From the 711 observations, 10% were used for validation, 10% for testing and 80% were used for training set. For the training algorithm, the division of data set were performed randomly. The training algorithm was scaled conjugate gradient and the performance were monitored by cross

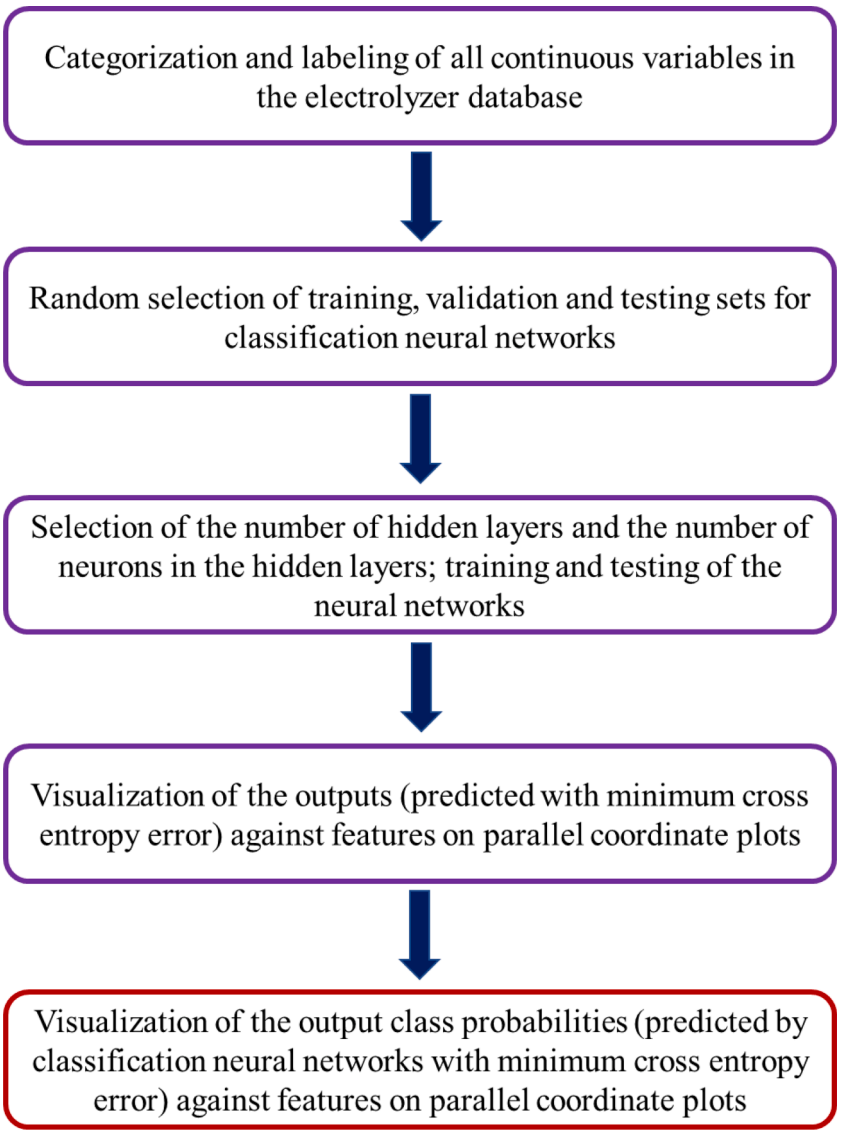

Fig. 6. Flow chart for neural network pattern recognition.

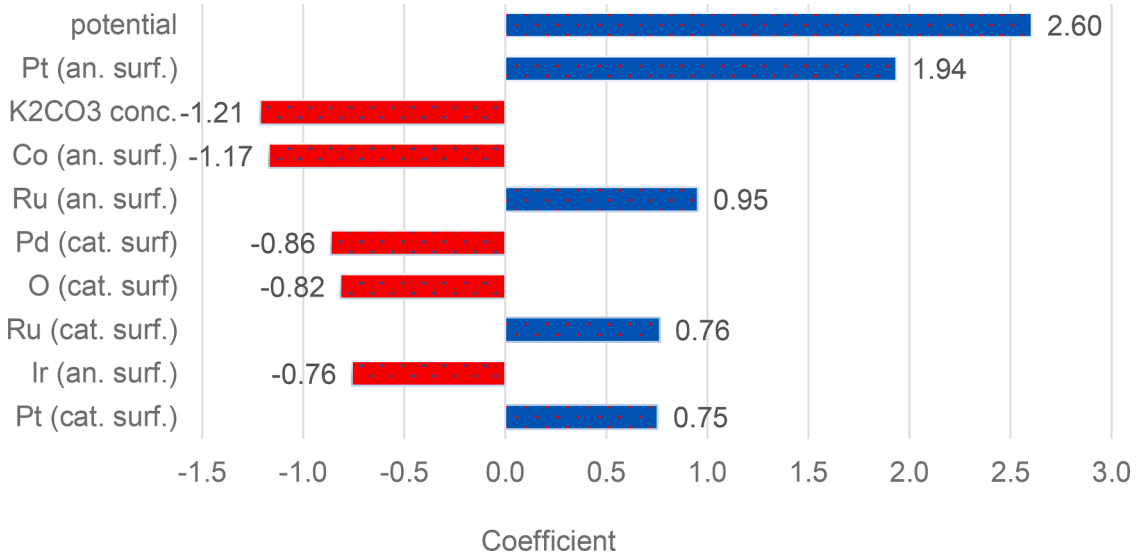

Fig. 7. Impact of top ten variables that contribute the most on current density.

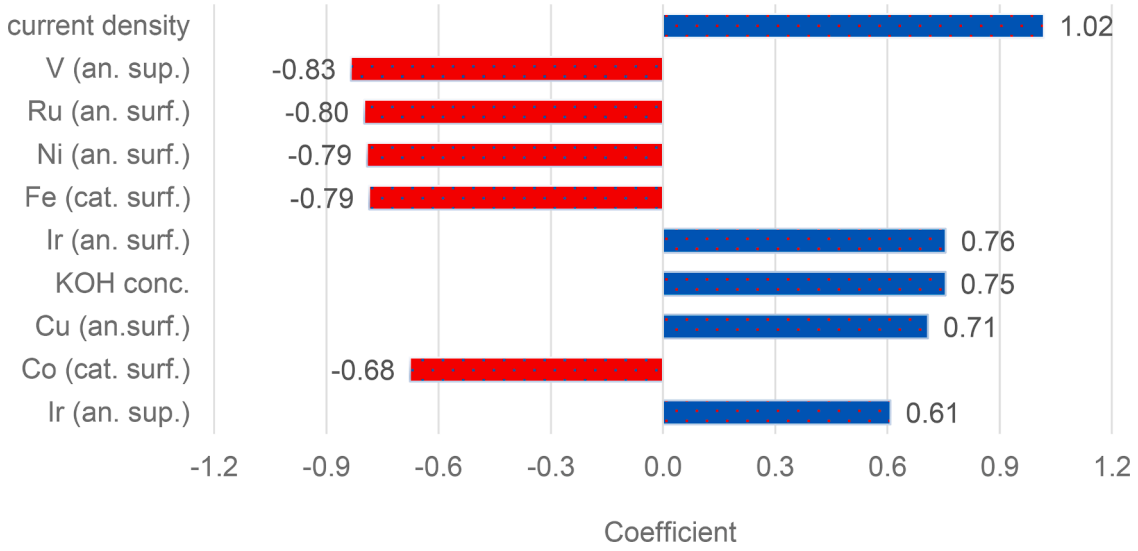

Fig. 8. Impact of top ten variables that contribute the most on polarization.

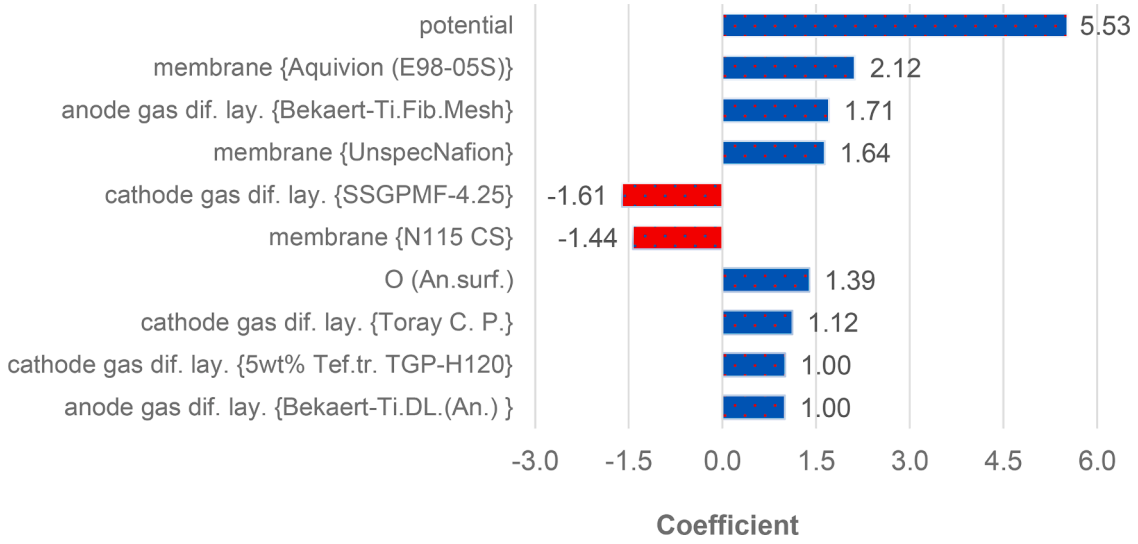

Fig. 9. Impact of top ten variables that contribute the most on power density.

entropy error (which is very common in neural networks). Cross entropy error can be shown with Eq. (1), where, n is the number of observations and C is the number of output classes and when t_{ic} is 1 if and only if sample i belongs to class c, and y_{ic} is the output probability that sample i belongs to class c.

$$-\sum_{i=1}^{n}\sum_{c=1}^{C} t_{ic}.\log(y_{ic}) \quad (1)$$

Neural Net Pattern Recognition Application in Matlab 2022a was used with the arranged data set described above. 711 observations were imported into the application to classify current density as low, medium and high ranges. Therefore, in the application, [292 x789] and [3x789] two dimensional arrays were used for descriptors and output (or responses). In the application the forward neural network is constructed with two layers which are hidden layer of 10 neurons and output layer which uses softmax transfer function. Softmax transfer function is used for classification neural networks. The number of neurons in the output layer is equal to the number of classes in the response data which is 3 (low, medium and high current density). The training of the model was performed until stopping criteria is met by monitoring the increase in validation error for six iterations (or epochs).

Table S1 shows cross-entropy and prediction errors for training, validation, testing sets at the end of training process. In addition, the trained model performance was also shown with cross-entropy and prediction errors of unseen data (additional test data). The results of neural network model were analyzed by confusion matrices Tables S2-S5 and parallel coordinates plots where high current density probability for all 292 layers were visualized.

3. Results and discussion

3.1. LIME

LIME methodology was applied as a part of explainable machine learning to determine the impact of each variable on the target variables. As it is described in Computational Details Section, the results were interpreted in such a way that a variable with a positive average coefficient affects the target positively, while a variable with a negative average coefficient affects it negatively. Moreover, the influence of a variable on performance is proportional to its average coefficients, with a bigger average coefficient indicating a stronger impact.

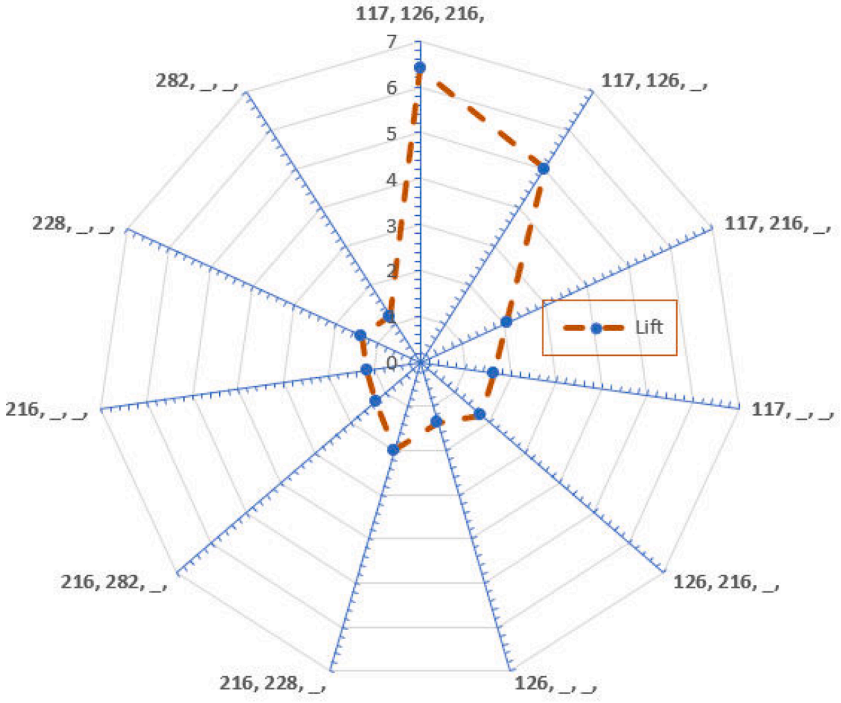

Layer #	Name of variable
282	T = 80°C
228	flowrate (ml/min) = 4
216	H_2O (concentration)(M) = 55.56
126	O (anode surface) = 0.67
117	Ir (anode surface) = 0.335
103	anode support to surface ratio = 0
67	ELAT (cathode gas diffusion layer)
23	Pt (cathode surface) = 1
18	cathode support to surface ratio = 24.39
11	C (cathode support) = 1

Fig. 10. Radar plots indicating importance of rules for high current density range.

Fig. 7 shows the top ten variables that contribute the most on current density. Accordingly, the increase of potential has the highest positive impact on the current density followed by the presence of Pt or Ru on the anode surface and the presence of Ru or Pt on the cathode surface. On the other hand, increasing the K_2CO_3 concentration in the electrolyte, adding Co or Ir on the anode surface and increasing Pd or O on the cathode surface have negative impact on the target. The impacts of all the variables on current density are given in detail in the supporting information.

The LIME method was also applied on polarization (Fig. 8) and power density (Fig. 9). For the polarization, current density was found to be the most important variable followed by a variety of anode/cathode support/surface variables. It was also found that the KOH concentration in the electrolyte has positive effect on polarization. For the power density, potential was determined as the variable that has the highest impact by far. Then, a variety of membranes, anode/cathode gas diffusion layers were found to be influential on the power density. Specifically, the effect of different types of membranes on power density may diversify. For instance, although N115 membrane exhibits negative coefficients (or negative effect) Aquivion membrane has just an opposite effect on performance. This positive effect of Aquivion membrane was linked to shorter side chain of the membrane bonded to sulfonate groups, high performance ionomer dispersion, low ohmic resistance, large crystalline structure, high glass transition temperature leading to low gas cross over and high thermal stability [45,46]. Similarly, the effect of all factors on polarization and power density is detailed in the supplementary information.

Interestingly, when the coefficients were analyzed for the three performance variables in Figs. 7–9, it was seen that the negatively affecting variables are all different for current, power density and polarization. It was also seen that the potential is the only common variable that is affecting power and current density positively. In addition, types of the most influential variables also differ for the performance variables though mostly cathode and anode surface elements affect current density and polarization. On the other hand, membrane and gas diffusion layer types are effective on power density. Therefore, it could be interpreted that in contrast to power density where material properties have dominant effect, current density and polarization are affected primarily by catalytic properties of electrodes.

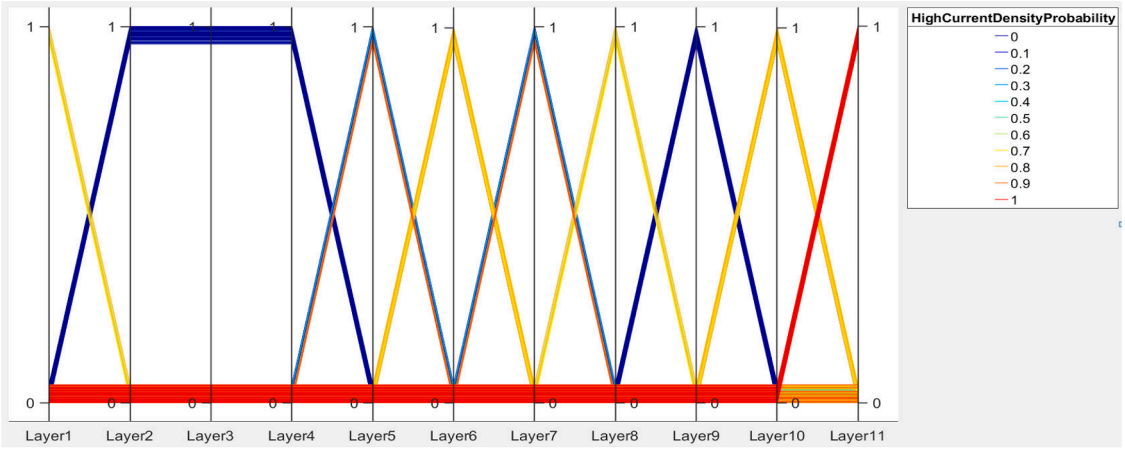

Descriptor variable	Ranges of continuous variables and identities of discrete variables
cathode support elements (layers 1-11)	(1) B:0.0708, (2) Ce:0.0043, (3) La:0.0022, (4) O:0.015, (5) Mo:0.335, (6) P:0.0099, (7) S:0.665, (8) C:0.9292, (9) C:0.98, (10) C:0.99, (11) C:1

Fig. 11. Parallel coordinate plots for layers 1-11.

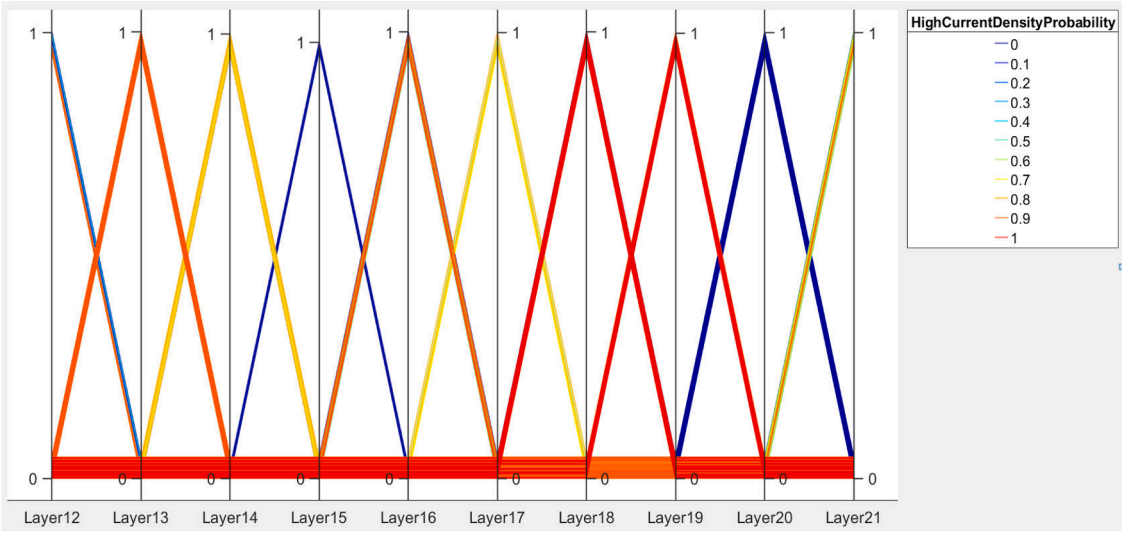

Descriptor variable	Ranges of continuous variables and identities of discrete variables
cathode support to surface ratio (layers 12-21)	(12) 4.76, (13) 10.84, (14) 12.83, (15) 16.26, (16) 19.08, (17) 20.84, (18) 24.39, (19) 37.93, (20) 39.38, (21) 65.03

Fig. 12. Parallel coordinate plots for layers 12-21.

3.2. *Association rule mining*

After execution and extraction of rules with lift values greater and equal to 1, all rules were visualized by radar plots. In the radar plots, each axis originating from the center of radar web shows range of lift values (with a minimum lift value of 1) and each lift axis correspond to different rules constructed of different layers of variables. For instance, Fig. 10 shows distribution of lift values among different rules which are combined of operational, catalytic and material variables. In addition, Fig. 10 also indicates that IrO_2 anode catalyst with pure water electrolyte gives the highest lift value. Although many surface elements were studied for anode electrode and although universal consensus would be to use ruthenium oxide for the anode, it is seen that Ir is a very important transition metal to achieve high performance [40,64,65]. The other radar plots in Figs S1–S5 indicate that most of the rules contain ELAT (cathode gas diffusion layer), cathode support to surface ratio: 24.39, pure Pt cathode surface, pure carbon cathode support and unsupported anode electrode.

3.3. *Neural network pattern recognition*

Finally, the effect of existence of each layer on the high current density probability was analyzed by paralel coordinate plots for the two layer classification neural network. Paralel coordinate plots are very useful for visualization of predictions (high current denstity probabilities) in relation with existence of different layers of catalytic, material and operational variables. Each paralel coordinate plot in this study shows ranges of high current density probabilities with different colors and 0 and 1 values in the layer axis shows absence or presence of that specific layer. In the paralel coordinate coordinate plots (from the output of neural network model), although mostly thick red color in the absence of layers was observed, it should be noted that the probability

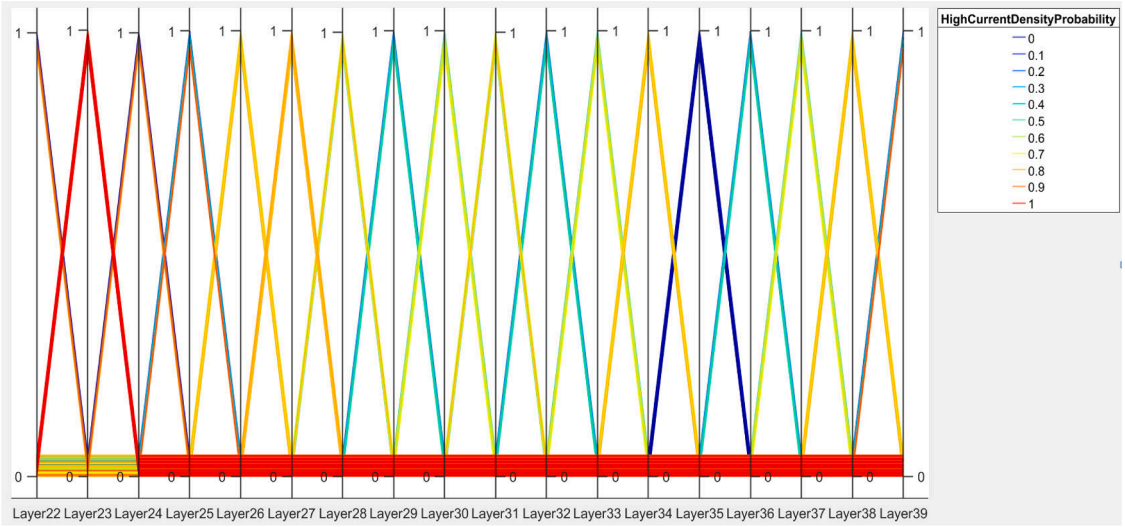

Descriptor variable	Ranges of continuous variables and identities of discrete variables
cathode surface elements (Layer 22-39)	(22) Pt:0.51, (23) Pt:1, (24) Ru:0.49, (25) Ru:0.335, (26) Al:0.66, (27) Pd:1, (28) O:0.571, (29) Fe:0.335, (30) Fe:0.33, (31) Co:0.43, (32) Co:0.335, (33) Co:0.33, (34) Mo:0.0717, (35) Ni:1, (36) Ni:0.335, (37) Ni:0.33, (38) Ni:0.269, (39) S:0.665

Fig. 13. Parallel coordinate plots for layers 22-39.

Table 2
Conditions of variables leading to high current densities from neural neural network pattern recognition.

Descriptor variable	Layer#	Conditions for high current density extracted from neural network pattern recognition
anode support to surface ratio	103, 104	0 (unsupported anode electrode), 1
anode surface elements	116, 117, 118, 119, 124, 126, 127, 150, 158, 159	Ir:0.33, Ir:0.335, Ir:0.42, Ir:0.7, Pt:0.34, O:0.67, O:0.66, Co:0.06, Ru:0.3, Ru:0.18
anode catalyst loading (mg. cm^{-2})	170, 172, 173, 183, 186	2.68, 2.2, 2, 0.51, 0.47
anode gas diffusion layer type	201, 202, 206, 207, 208, 210, 215	Ti Felt, PTL 4 - Fibrous Ti-Sinter (porosity % 67.61), titanium Fibre Mesh (Bekaert Toko Metal Fiber Co.), Ir coated Bekipor® ST Titanium Grade 1 felts with 68% porosity, Pt Coated Titanium Fibre Mesh, porous titanium disc made of sintered powder (APT Co.), TGPH-120 Toray
electrolyte type	216, 217	H_2O (concentration) (M): 55.56, H_2O (concentration) (M): 55.55
flowrate of electrolytes ($ml.min^{-1}$)	225, 227, 228, 230, 231, 232, 235	1, 3.30, 4, 25, 40, 50, 500
membrane type	236,237,240,242,243,244,246	Aqivion (E98-09S), Aquivion (E98-05S), Aqivion (E100-09S), N115, N115CS, N117, Nafion membrane (model unspecified),
potential (V)	260, 261, 262, 263	2.1, 2, 1.9, 1.8
temperature (^oC)	280, 281, 282, 283, 284, 285, 286	110, 90, 80, 70, 60, 55, 50

values in the presence of layers gives information about the possible performance condition when that layer is applied in the electrolyzer and in addition, high probabilities in the absence of layers could be interpreted as dominance of other layers on the high performance seperately.

Fig. 11 shows the effect of cathode support elements at certain mole fractions used in the scientific literature. It is seen in this figure that pure carbon support has the highest probability for high current density. Parallel coordinate plots also helped us to search for optimum conditions, unique layers leading to high performance or the characteristics of different type of catalytic or operational variables. For instance, as seen in Fig. 12, unlike cathode support elements, there is no unique cathode support to surface ratio leading to high current density.

Interestingly, as seen in Fig. 13, similiar results to ARM were also extracted in pattern recognition like condition of pure Pt on cathode surface for high current density. The other parallel coordinate plots in Figs. S6–S8 indicate that there is no single cathode loading ,gas diffusion layer for high performance, anode support element (C or Ti). For the rest of the paralel coordinate plots in Figs. S9–S16, the descriptor variables and the condition of variable leading to high current densities were tabulated as seen in Table 2.

4. Conclusions

In this work, three innovative machine learning algorithms were utilized for the objective of detecting relevant factors and exploring routes leading to high performance in PEM and AEM electrolyzers. First, LIME methodology indicated positive effect of certain variables on the performance like Pt, Ru anode surface elements, K_2CO_3 or KOH concentration in the electrolyte or certain membrane types and gas diffusion layers, etc. Secondly, the rules for high performance extracted from ARM showed that the rules were dominated by ELAT (cathode gas diffusion layer), cathode support to surface ratio: 24.39, pure Pt cathode surface, pure carbon cathode support and unsupported anode. Finally, neural network pattern recognition model with low cross entropy and prediction error showed catalytic or operational variables with highest probability for high performance like pure carbon support on cathode or the existence of certain anode surface elements with certain mole fractions (Pt, Ir, Co, O, Ru) or certain applied potential (above 1.8V) etc. We believe that the constantly evolving machine learning field with fresh

methodologies will always provide new doors for PEM and AEM electrolyzers, and this may help guide future research in hydrogen production.

Declaration of Competing Interest

The authors declare that they have no known competing financial interests or personal relationships that could have appeared to influence the work reported in this paper.

Data availability

Data will be made available on request.

Supplementary materials

Supplementary material associated with this article can be found, in the online version, at doi:10.1016/j.egyai.2023.100254.

References

[1] Dellosa JT, Palconit EC. Artificial Intelligence (AI) in renewable energy systems: a condensed review of its applications and techniques. In: Proceedings of the IEEE international conference on environment and electrical engineering and 2021 IEEE industrial and commercial power systems Europe (EEEIC /I&CPS Europe); 2021. p. 1–6.

[2] Erdem Günay M, Yıldırım R. Recent advances in knowledge discovery for heterogeneous catalysis using machine learning. Catal Rev 2020;63(1):120–64. https://doi.org/10.1080/01614940.2020.1770402.

[3] Bannor BE, Acheampong AO. Deploying artificial neural networks for modeling energy demand: international evidence. Int J Energy Sect Manag 2019;14(2): 285–315. https://doi.org/10.1108/ijesm-06-2019-0008.

[4] Liu X, Moreno B, García AS. A grey neural network and input-output combined forecasting model. Primary energy consumption forecasts in Spanish economic sectors. Energy 2016;115:1042–54. https://doi.org/10.1016/j.energy.2016.09.017.

[5] Panapakidis IP, Dagoumas AS. Day-ahead natural gas demand forecasting based on the combination of wavelet transform and ANFIS/genetic algorithm/neural network model. Energy 2017;118:231–45. https://doi.org/10.1016/j.energy.2016.12.033.

[6] Sen D, Tunç KMM, Günay ME. Forecasting electricity consumption of OECD countries: a global machine learning modeling approach. Utilities Policy 2021:70. https://doi.org/10.1016/j.jup.2021.101222.

[7] Szoplik J. Forecasting of natural gas consumption with artificial neural networks. Energy 2015;85:208–20. https://doi.org/10.1016/j.energy.2015.03.084.

[8] Al-Musaylh MS, et al. Short-term electricity demand forecasting with MARS, SVR and ARIMA models using aggregated demand data in Queensland, Australia. Adv Eng Inf 2018;35:1–16. https://doi.org/10.1016/j.aei.2017.11.002.

[9] Kaytez F. A hybrid approach based on autoregressive integrated moving average and least-square support vector machine for long-term forecasting of net electricity consumption. Energy 2020;197. https://doi.org/10.1016/j.energy.2020.117200.

[10] Sohani A, et al. Using machine learning in photovoltaics to create smarter and cleaner energy generation systems: a comprehensive review. J Clean Prod 2022: 364. https://doi.org/10.1016/j.jclepro.2022.132701.

[11] Zhao E, Sun S, Wang S. New developments in wind energy forecasting with artificial intelligence and big data: a scientometric insight. Data Sci Manag 2022;5 (2):84–95. https://doi.org/10.1016/j.dsm.2022.05.002.

[12] Okoroafor ER, et al. Machine learning in subsurface geothermal energy: two decades in review. Geothermics 2022:102. https://doi.org/10.1016/j.geothermics.2022.102401.

[13] Wang Z, et al. The role of machine learning to boost the bioenergy and biofuels conversion. Bioresour Technol 2022;343:126099. https://doi.org/10.1016/j.biortech.2021.126099.

[14] Faizollahzadeh Ardabili S, et al. Computational intelligence approach for modeling hydrogen production: a review. Eng Appl Comput Fluid Mech 2018;12(1):438–58. https://doi.org/10.1080/19942060.2018.1452296.

[15] Abdin Z, et al. Hydrogen as an energy vector. Renew Sustain Energy Rev 2020;120. https://doi.org/10.1016/j.rser.2019.109620.

[16] Amin M, et al. Hydrogen production through renewable and non-renewable energy processes and their impact on climate change. Int J Hydrog Energy 2022;47(77): 33112–34. https://doi.org/10.1016/j.ijhydene.2022.07.172.

[17] Günay ME, Tapan NA, Akkoç G. Analysis and modeling of high-performance polymer electrolyte membrane electrolyzers by machine learning. Int J Hydrog Energy 2022;47(4):2134–51. https://doi.org/10.1016/j.ijhydene.2021.10.191.

[18] Falcão DS, Pinto AMFR. A review on PEM electrolyzer modelling: Guidelines for beginners. J Clean Prod 2020:261. https://doi.org/10.1016/j.jclepro.2020.121184.

[19] Ding R, et al. Machine learning utilized for the development of proton exchange membrane electrolyzers. J Power Sources 2023:556. https://doi.org/10.1016/j.jpowsour.2022.232389.

[20] Zhao D, et al. Dynamic hierarchical modeling and control strategy of high temperature proton exchange electrolyzer cell system. Int J Hydrog Energy 2022; 47(53):22302–15. https://doi.org/10.1016/j.ijhydene.2022.05.067.

[21] Mohamed A, Ibrahem H, Kim K. Machine learning-based simulation for proton exchange membrane electrolyzer cell. Energy Rep 2022;8:13425–37. https://doi.org/10.1016/j.egyr.2022.09.135.

[22] Yin H, et al. Machine learning for membrane design and discovery. Green Energy & Environment; 2022. https://doi.org/10.1016/j.gee.2022.12.001.

[23] Kim S, Kim J, Kim DK. Understanding operating characteristics of polymer electrolyte membrane water electrolyzer for developing optimal machine learning techniques. In: Proceedings of the 13th international conference on information and communication technology convergence (ICTC); 2022. p. 1056–8.

[24] Khan MA, et al. Recent progresses in electrocatalysts for water electrolysis. Electrochem Energy Rev 2018;1(4):483–530. https://doi.org/10.1007/s41918-018-0014-z.

[25] Ito H, et al. Experimental investigation of electrolytic solution for anion exchange membrane water electrolysis. Int J Hydrog Energy 2018;43(36):17030–9. https://doi.org/10.1016/j.ijhydene.2018.07.143.

[26] Ito H, et al. Investigations on electrode configurations for anion exchange membrane electrolysis. J Appl Electrochem 2018;48(3):305–16. https://doi.org/10.1007/s10800-018-1159-5.

[27] Tang C, et al. Ni3S2 nanosheets array supported on Ni foam: a novel efficient three-dimensional hydrogen-evolving electrocatalyst in both neutral and basic solutions. Int J Hydrog Energy 2015;40(14):4727–32. https://doi.org/10.1016/j.ijhydene.2015.02.038.

[28] Vincent I, Lee EC, Kim HM. Highly cost-effective platinum-free anion exchange membrane electrolysis for large scale energy storage and hydrogen production. RSC Adv 2020;10(61):37429–38. https://doi.org/10.1039/d0ra07190k.

[29] Wu X, Scott K. A Li-doped Co3O4 oxygen evolution catalyst for non-precious metal alkaline anion exchange membrane water electrolysers. Int J Hydrog Energy 2013; 38(8):3123–9. https://doi.org/10.1016/j.ijhydene.2012.12.087.

[30] Xu D, et al. Earth-abundant oxygen electrocatalysts for alkaline anion-exchange-membrane water electrolysis: effects of catalyst conductivity and comparison with performance in three-electrode cells. ACS Catal 2018;9(1):7–15. https://doi.org/10.1021/acscatal.8b04001.

[31] Bates MK, et al. Composite Ni/NiO-Cr(2)O(3) catalyst for alkaline hydrogen evolution reaction. J Phys Chem C Nanomater Interfaces 2015;119(10):5467–77. https://doi.org/10.1021/jp512311c.

[32] Hong SH, et al. High-activity electrodeposited NiW catalysts for hydrogen evolution in alkaline water electrolysis. Appl Surf Sci 2015;349:629–35. https://doi.org/10.1016/j.apsusc.2015.05.040.

[33] McKone JR, et al. Ni–Mo nanopowders for efficient electrochemical hydrogen evolution. ACS Catal 2013;3(2):166–9. https://doi.org/10.1021/cs300691m.

[34] Tajuddin AAH, et al. Corrosion-resistant non-noble metal electrodes for PEM-type water electrolyzer. Int J Hydrog Energy 2021;46(78):38603–11. https://doi.org/10.1016/j.ijhydene.2021.09.116.

[35] Chourashiya MG, Urakawa A. Solution combustion synthesis of highly dispersible and dispersed iridium oxide as an anode catalyst in PEM water electrolysis. J Mater Chem A 2017;5(10):4774–8. https://doi.org/10.1039/c6ta11047a.

[36] Hao C, et al. Investigation of V-doped TiO2 as an anodic catalyst support for SPE water electrolysis. Int J Hydrog Energy 2017;42(15):9384–95. https://doi.org/10.1016/j.ijhydene.2017.02.131.

[37] Kumar, S.V.K. A survey on association rule mining. 2013.

[38] Kúš P, et al. Magnetron sputtered Ir thin film on TiC-based support sublayer as low-loading anode catalyst for proton exchange membrane water electrolysis. Int J Hydrog Energy 2016;41(34):15124–32. https://doi.org/10.1016/j.ijhydene.2016.06.248.

[39] Lettenmeier P, et al. Nanosized IrO(x)-Ir catalyst with relevant activity for anodes of proton exchange membrane electrolysis produced by a cost-effective procedure. Angew Chem Int Ed Engl 2016;55(2):742–6. https://doi.org/10.1002/anie.201507626.

[40] Liu C, et al. Performance enhancement of PEM electrolyzers through iridium-coated titanium porous transport layers. Electrochem Commun 2018;97:96–9. https://doi.org/10.1016/j.elecom.2018.10.021.

[41] Mazúr P, et al. Non-conductive TiO2 as the anode catalyst support for PEM water electrolysis. Int J Hydrog Energy 2012;37(17):12081–8. https://doi.org/10.1016/j.ijhydene.2012.05.129.

[42] Natarajan V, Basu S. Performance and degradation studies of RuO2–Ta2O5 anode electrocatalyst for high temperature PBI based proton exchange membrane water electrolyser. Int J Hydrog Energy 2015;40(46):16702–13. https://doi.org/10.1016/j.ijhydene.2015.07.041.

[43] Rozain C, et al. Influence of iridium oxide loadings on the performance of PEM water electrolysis cells: Part II – Advanced oxygen electrodes. Appl Catal, B 2016; 182:123–31. https://doi.org/10.1016/j.apcatb.2015.09.011.

[44] Sarno M, Ponticorvo E. High hydrogen production rate on RuS2@MoS2 hybrid nanocatalyst by PEM electrolysis. Int J Hydrog Energy 2019;44(9):4398–405. https://doi.org/10.1016/j.ijhydene.2018.10.229.

[45] Siracusano S, et al. The influence of iridium chemical oxidation state on the performance and durability of oxygen evolution catalysts in PEM electrolysis. J Power Sources 2017;366:105–14. https://doi.org/10.1016/j.jpowsour.2017.09.020.

[46] Siracusano S, et al. Enhanced performance and durability of low catalyst loading PEM water electrolyser based on a short-side chain perfluorosulfonic ionomer. Appl Energy 2017;192:477–89. https://doi.org/10.1016/j.apenergy.2016.09.011.
[47] Slavcheva E, et al. Ebonex supported iridium as anode catalyst for PEM water electrolysis. Int J Hydrog Energy 2015;40(35):11356–61. https://doi.org/10.1016/j.ijhydene.2015.03.005.
[48] Günay ME, Tapan NA. Evaluation of polymer electrolyte membrane electrolysis by explainable machine learning, optimum classification model, and active learning. J Appl Electrochem 2022. https://doi.org/10.1007/s10800-022-01786-8.
[49] Ribeiro MT, Singh S, Guestrin C. "Why should i trust you?". In: Proceedings of the 22nd ACM SIGKDD international conference on knowledge discovery and data mining; 2016. p. 1135–44.
[50] Benk M, Ferrario A. Explaining interpretable machine learning: theory, methods and applications. SSRN Electron J 2020. https://doi.org/10.2139/ssrn.3748268.
[51] Garreau, D. and U. von Luxburg Explaining the explainer: a first theoretical analysis of LIME. 2020. 10.48550/arXiv.2001.03447.
[52] Ribeiro, M.T., S. Singh, and C. Guestrin Model-agnostic interpretability of machine learning. 2016. 10.48550/arXiv.1606.05386.
[53] Molnar C. Interpretable Machine Learning: a Guide for Making Black Box Models Explainable. 2 ed. ↑Independently published; 2022.
[54] Togacar M, et al. Detection of COVID-19 findings by the local interpretable model-agnostic explanations method of types-based activations extracted from CNNs. Biomed Signal Process Control 2022;71:103128. https://doi.org/10.1016/j.bspc.2021.103128.
[55] Solanki SK, Patel J. A survey on association rule mining. In: Proceedings of the fifth international conference on advanced computing & communication technologies; 2015. p. 212–6.
[56] Tapan NA, Günay ME, Yıldırım N. Application of machine learning for the determination of damaged starch ratio as an alternative to medcalf and gilles principle. Food Anal Methods 2022. https://doi.org/10.1007/s12161-022-02442-9.
[57] Ai D, et al. Association rule mining algorithms on high-dimensional datasets. Artif Life Robot 2018;23(3):420–7. https://doi.org/10.1007/s10015-018-0437-y.
[58] Yegnanarayana B. Artificial neural networks for pattern recognition. Sadhana 1994;19(2):189–238. https://doi.org/10.1007/bf02811896.
[59] Martin ST, Morrison CL, Hoffmann MR. Photochemical mechanism of size-quantized vanadium-doped TiO2 particles. J Phys Chem 2002;98(51):13695–704. https://doi.org/10.1021/j100102a041.
[60] Bhattacharyya K, et al. Mechanistic insight by *in situ* FTIR for the gas phase photo-oxidation of ethylene by V-doped titania and nano titania. J Phys Chem B 2009;113(17):5917–28. https://doi.org/10.1021/jp8103529.
[61] Hahsler M, Grün B, Hornik K. arules - A computational environment for mining association rules and frequent item sets. J Stat Softw 2005;14(15):1–25. https://doi.org/10.18637/jss.v014.i15.
[62] Hussein N, Alashqur A, Sowan B. Using the interestingness measure lift to generate association rules. J Adv Comput Sci Technol 2015;4(1). https://doi.org/10.14419/jacst.v4i1.4398.
[63] Malone, J., ARMADA Data Mining Tool 2022, MATLAB Central File Exchange.
[64] Bernt M, Gasteiger HA. Influence of Ionomer Content in IrO2/TiO2Electrodes on PEM Water Electrolyzer Performance. J Electrochem Soc 2016;163(11):F3179–89. https://doi.org/10.1149/2.0231611jes.
[65] Yu H, et al. Nano-size IrOx catalyst of high activity and stability in PEM water electrolyzer with ultra-low iridium loading. Appl Catal B 2018;239:133–46. https://doi.org/10.1016/j.apcatb.2018.07.064.